Vortex dynamics in superfluid helium films

P. W. Adams* and W. I. Glaberson
Serin Physics Laboratory, Rutgers University, Piscataway, New Jersey 08854
(Received 31 July 1986)

A high-Q torsional oscillator was used to measure the superfluid density and excess dissipation in thin films of ^{4}He as a function of temperature and film thickness. The effects of rotation on the Kosterlitz-Thouless transition were studied and the rotation-induced dissipation was measured. The first direct measurements of vortex diffusivity D as a function of the temperature through the superfluid transition were obtained. We find that D is a rapidly varying function of temperature in the vicinity of the transition. It is very small well below the transition, increases to order $\hbar/m$ at the static transition temperature, and appears to diverge at the point where the superfluid density vanishes. The diffusivity also appears to be insensitive to the presence of ^{3}He impurities and to the nature of the substrate.

I. INTRODUCTION

In recent years there has been a great deal of interest in two-dimensional (2D) superconducting and superfluid ^{4}He systems. In these systems, thermally activated defects (i.e., vortex-antivortex pairs) are the dominant fluctuations and mediate the transition to the respective superconducting and superfluid phases. The static theory of these 2D phase transitions, which fall in the same universality class as the XY model,[1] has been a great success. The theory, first developed by Kosterlitz and Thouless,[2] associates the transition from the superfluid to the normal phase with the unbinding of thermal vortex-antivortex pairs at the static transition temperature $T_{\rm KT}$. This unbinding is a cooperative effect which destroys the algebraic long-range order of the system at a nonzero superfluid density predicted by the theory.[3]

Kosterlitz and Thouless[2] used renormalization-group techniques to solve the problem of a dilute gas of logarithmically interacting vortex-antivortex pairs. By considering the effects of smaller pairs on the interaction between the members of larger pairs, they were able to extract a scale-dependent dielectric constant and vortex-pair-excitation probability. The scale dependence of these parameters is given by the Kosterlitz-Thouless recursion relations. For an unbounded experiment carried out at zero frequency, the recursion relations are iterated to infinite scale. The transition temperature is defined as the largest temperature for which the vortex-excitation probability no longer vanishes at infinite scale (i.e., infinite pair separation).

To interpret experiments at finite frequencies, the Kosterlitz-Thouless static theory must be incorporated into a more comprehensive theory that accounts for the dynamic response of the vortex plasma to an oscillating field. Ambegaokar and Teitel[4] have shown that the vortex-diffusion length r_D is the characteristic separation beyond which pairs can no longer equilibrate to the external field. This leads to two modifications of the static theory.[5] First, because pairs larger than r_D do not participate in the renormalization, the Kosterlitz-Thouless recursion relations are not iterated out to infinite scale but to a finite cutoff. This, in effect, shifts the transition temperature up from $T_{\rm KT}$ to a new frequency-dependent dynamic transition temperature T_c. Second, the effective dielectric constant becomes complex to account for dissipative vortex motion.

Since r_D is, by definition, proportional to the square root of diffusivity, it is apparent that D is the primary transport parameter of this theory and is of fundamental interest. In this paper, we report the results of an investigation of the effects of rotation on the Kosterlitz-Thouless transition in thin films of ^{4}He and present direct measurements of D as a function of temperature through the transition. A brief discussion of these results has been published.[6]

II. THEORY AND PREVIOUS EXPERIMENTS

A. 2D superfluidity

It has been known for a long time that thermal fluctuations (i.e., phonons, spin waves, etc.) become important in 2D systems and that these fluctuations can destroy the long-range order commonly observed in their three-dimensional (3D) counterparts. As far back as 1930, Bloch[7] showed that there is no finite spontaneous magnetization in 2D magnetic lattices at nonzero temperatures. Peierls[8] showed in 1935 that there can be no long-range order in one- or two-dimensional crystals at finite temperatures. Finally, in 1967, Hohenberg[9] provided a rigorous proof that the superfluid order parameter is destroyed in two or fewer dimensions, at finite temperatures.

This somewhat overwhelming theoretical evidence for the absence of superfluidity in two dimensions is, however, in conflict with many experimental results. Superfluid flow in thin films of helium had been observed as far back as 1940 by Long and Meyer.[10] The rate of heat transfer in unsaturated films was measured by Bowers *et al.*[11] in 1951. Their data displayed superfluid character and showed that the λ point was suppressed in thin films. The first solid evidence of superfluid behavior came from

third-sound measurements in which temperature waves were propagated in thin films of helium.[12] The third-sound measurements of Rudnick[13] in the late 1970s showed clear evidence of a superfluid transition. Finally, in 1978, Bishop and Reppy[14] used an oscillating substrate method to provide the first quantitative characterization of the superfluid transition in thin films of helium.

The apparent discrepancy between theory and experiment raises the question as to whether or not one can define a "superfluid" density for a system for which there is no traditional long-range order. To answer this question, one starts by defining a local condensate wave function which is analogous to the 3D wave function,

$$\Psi(r)=|\psi(r)|e^{i\phi(r)} . \tag{2.1}$$

Now if the spatial variations of the amplitude of the wave function are on a sufficiently large scale, then well below T_λ, only fluctuations in its phase will be important, in which case the effective Hamiltonian can be written as

$$H=\frac{\hbar^2 n(T)}{2m}\int(\nabla\phi)^2 d^2r , \tag{2.2}$$

where $n(T)$ is the number density of helium atoms in the condensate. The areal superfluid density σ_s is analogous to the spin-wave stiffness constant in magnetic systems and can be defined as[1]

$$(\sigma_s)^{-1}=\left[\frac{\hbar^2}{m^2kT}\right]\int d^2r\langle\nabla\phi(r)\cdot\nabla\phi(0)\rangle . \tag{2.3}$$

(It is beyond the scope of this paper to discuss the relationship between the condensate and the superfluid fraction—for the purposes of the present discussion we will blur the distinction.) If a Gaussian form of Eq. (2.2) is used then the expectation value in Eq. (2.3) is easily evaluated and we find that

$$\sigma_s=mn(T) . \tag{2.4}$$

Thus, though no long-range order exists in these 2D XY systems, it is possible to define an effective superfluid density which may display many of the characteristics of 3D superfluidity.

The role of dimensionality in superfluid behavior is more clearly seen by defining the correlation function,

$$G(r)=\langle\Psi(r)\Psi^*(0)\rangle . \tag{2.5}$$

In three dimensions, if there is no long-range order then $G(r)$ decays exponentially

$$G(r)\propto\exp[-r/\xi(T)] , \tag{2.6}$$

where $\xi(T)$ is a temperature-dependent correlation length. This is clearly the case for liquid helium above T_λ. He II exhibits long-range order in momentum space which can be represented by a ground-state condensate wave function which is phase correlated throughout the fluid

$$\langle\Psi(r)\rangle\propto\sqrt{\rho}e^{i\phi(r)} \tag{2.7}$$

where ρ is the condensate number density. The phase correlation breaks the symmetry of the noncorrelated wave function and leads to a nonzero asymptotic value for $G(r)$,

$$\lim_{r\to\infty}G(r)=\text{const}\neq 0 . \tag{2.8}$$

In two dimensions, the thermal fluctuations previously discussed can lead[1] to an algebraic decay in $G(r)$—very similar to that observed in 3D systems near a critical point,

$$G(r)\propto\frac{1}{r^{\eta(T)}} \tag{2.9}$$

where $\eta(T)$ is a nonuniversal temperature-dependent exponent. This type of system is said to have "algebraic long-range order" and displays superfluid behavior.

B. Kosterlitz-Thouless theory

As outlined above, phase fluctuations in the condensate wave function are energetically favored over amplitude fluctuations in 2D systems. This fact leads to algebraic decay in the order parameter which is believed to be a general characteristic of 2D superfluidity. Kosterlitz and Thouless[2] identified the primary mechanism for such fluctuations [which is not included in the simple-phase Hamiltonian of Eq. (2.2)]. They predicted that vortex-antivortex pair excitations would dominate the fluctuations at sufficiently high temperatures and could in fact destroy the algebraic long-range order of the system. They used a simple free-energy argument to demonstrate this possibility. The energy of a single isolated vortex in a system of dimension L is easily found to be[15]

$$E=\frac{\pi\hbar^2\sigma_s^0}{m^2}\ln(L/r_0) , \tag{2.10}$$

where r_0 is the vortex core radius and σ_s^0 is the unrenormalized areal superfluid density. The entropy associated with such an excitation is obtained by noting that there are $N=(L/r_0)^2$ places in which the vortex can be placed. The entropy is therefore

$$\begin{aligned}S&=k\ln(N)\\&=2k\ln(L/r_0) .\end{aligned} \tag{2.11}$$

Since both the entropy and the energy scale as $\ln(L/r_0)$, it is clear that the free energy of a vortex excitation $F=E-TS$ changes sign at a well-defined temperature

$$T_{\mathrm{KT}}=\frac{\pi\hbar^2\sigma_s^0}{2m^2k} . \tag{2.12}$$

Below T_{KT}, the energy term dominates F and vortex excitations are suppressed. Above T_{KT}, the entropy term dominates and thermally activated free vortices will spontaneously appear in the system—destroying the phase coherence.

The energy required to create an isolated vortex Eq. (2.10) is much greater than that required to create a vortex-antivortex pair E_c. Thus a thermally activated pair is much more likely to appear than a single isolated vortex. It is easily shown that the energy of a rectilinear pair varies logarithmically in pair separation r,

$$E_p = 2\pi\sigma_s^0 \left[\frac{\hbar}{m}\right]^2 \ln(r/r_0) + E_c \ . \tag{2.13}$$

This is a long-range interaction which can lead to dramatic cooperative effects in a many-body system.

Kosterlitz and Thouless used renormalization techniques to solve the statistical problem of a 2D gas of logarithmically interacting vortex-antivortex pairs. They accounted for the attenuating effect of smaller pairs on the interaction between the respective members of larger pairs by introducing a scale dependent dielectric constant $\tilde{\epsilon}$ into Eq. (2.13). A large test pair polarizes the intervening pair plasma which in turn screens some of the bare interaction. The resulting effective interaction can be written as

$$E_p = 2\pi\sigma_s^0 \left[\frac{\hbar}{m}\right]^2 \int_{r_0}^{r} \frac{dr'}{r'\tilde{\epsilon}(r')} + E_c \ . \tag{2.14}$$

Note that Eq. (2.14) is logarithmic in r/r_0 when $\tilde{\epsilon}=1$. To obtain a self-consistent determination of $\tilde{\epsilon}(r)$, one starts with the general relation between $\tilde{\epsilon}$ and the susceptibility $\chi(r)$,

$$\tilde{\epsilon}(r) = 1 + 4\pi\chi(r) \ . \tag{2.15}$$

The susceptibility is related to the polarizability $\alpha(r)$ by

$$\chi(r) = \int_{r_0}^{r} \alpha(r')dn(r') \ , \tag{2.16}$$

where $n(r)$ is the number density of pairs. Equations (2.15) and (2.16) can, in principle, be used to determine $\tilde{\epsilon}(r)$ once $\alpha(r)$ and $n(r)$ are known.

The polarizability per pair of a charged plasma is given by

$$\alpha(r) = q\frac{\partial}{\partial E}\langle r\cos\theta\rangle \mid_{E=0} \ , \tag{2.17}$$

where q is the charge of a pair member, E is the applied electric field, and θ is the angle between the dipole moment and E. This system is analogous to the vortex-pair system with the following transcription:

$$\begin{aligned} &2q^2 \rightleftarrows 2\pi\sigma_s^0 \left[\frac{\hbar}{m}\right]^2 \ , \\ &q\mathbf{E} \rightleftarrows 2\pi\sigma_s^0 \frac{\hbar}{m}\hat{\mathbf{z}}\times(\mathbf{V}_n - \mathbf{V}_s) \ , \end{aligned} \tag{2.18}$$

where $\mathbf{v}_n$ and $\mathbf{v}_s$ are the normal fluid and superfluid velocities, respectively. Equation (2.17) can easily be evaluated by assuming that the field giving rise to the polarization (i.e., the field of the large test pair) is relatively constant over the dipole pairs. Under this assumption, the differentiation with respect to E and the limit $E\rightarrow 0$ can be performed before integrating out the thermal average. After carrying out the differentiation and the limit, we can easily evaluate the average over the Boltzmann factor,

$$\begin{aligned} \exp[-E_p(r)/kT] = (r/r_0)^{2q^2/kT\tilde{\epsilon}} &\exp(Eqr\cos\theta/kT) \\ &\times\exp(-E_c/kT) \end{aligned} \tag{2.19}$$

in which case

$$\alpha(r) = \frac{q^2r^2}{2kT} \tag{2.20}$$

which translates to

$$\alpha(r) = \frac{\pi K_0 r^2}{2} \tag{2.21}$$

in the 2D helium system, where

$$K_0 = \sigma_s^0 \left[\frac{\hbar}{m}\right]^2 \Big/ kT \ . \tag{2.22}$$

The probability P of a pair existing in an area L^2 is equal to the sum of

$$\exp[-E_p(\mid \mathbf{r}_i - \mathbf{r}_j \mid /r_0)/kT] \tag{2.23}$$

over all possible $\mathbf{r}_i$ and $\mathbf{r}_j$. We can transform the sum into a double integral by assuming that $\exp(-E_c/kT) \ll 1$ and simply counting the possible configurations. There are $(L/r_0)^2$ possible locations for the first pair member and $2\pi r dr/r_0^2$ possible locations for the second in an annulus with radius r and width dr. Therefore,

$$dP(r) = \frac{L^2}{r_0^2}\left[\frac{2\pi r dr}{r_0^2}\exp[-E_p(r)/kT]\right] \tag{2.24}$$

and we identify

$$dn(r) = dP(r)/L^2 \tag{2.25}$$

in which case Eq. (2.16) becomes

$$\chi(r) = \int_{r_0}^{r} \alpha(r)\exp[-E_p(r)/kT]\frac{2\pi r dr}{r_0^4} \ . \tag{2.26}$$

Equations (2.15) and (2.26) can now be combined for a self-consistent determination of the effective interaction. The result is the famous Kosterlitz-Thouless recursion relations from which a scale dependent dielectric constant $\tilde{\epsilon}$ and vortex-pair-excitation probability y^2 can be extracted

$$\begin{aligned} &K^{-1}(l) = K_0^{-1} + 4\pi^3 \int_0^l y^2(l')dl' \ , \\ &y^2(l) = y_0^2 \exp\left[4l - 2\pi\int_0^l K(l')dl'\right] \ , \end{aligned} \tag{2.27}$$

where

$$\begin{aligned} &l = \ln(r/r_0) \ , \\ &K^{-1}(l) = \tilde{\epsilon}(l)/K_0 \ , \\ &y_0^2 = \exp(-E_c/kT) \ . \end{aligned} \tag{2.28}$$

The measured superfluid density σ_s in this theory is

$$\sigma_s = \sigma_s^0(T)/\tilde{\epsilon} \ , \tag{2.29}$$

where $\sigma_s^0(T)$ is the temperature-dependent background areal superfluid density—of order $\rho_s(T)h$, where h is the film thickness. The vortex-excitation probability y^2 is related to the density of pairs per unit area of separation $\delta n(r)$ by

$$\delta n(r) = \frac{y^2(r)}{r^4} \ . \tag{2.30}$$

In principle, the recursion relations of Eqs. (2.27) can be used to predict the static Kosterlitz-Thouless transition in an unbounded system by iterating them to $l=\infty$ from a

locus of initial conditions

$$y^2(l=0,T)=y_0^2(T)\ ,$$
$$K(l=0,T)=K_0(T)\ . \tag{2.31}$$

The static transition temperature $T_{\rm KT}$ is defined as the smallest temperature for which

$$\lim_{l\to\infty} y^2(l,T_{\rm KT})\neq 0 \tag{2.32}$$

or equivalently by

$$\lim_{l\to\infty} \tilde{\epsilon}(l,T_{\rm KT})=\pi K_0/2 \tag{2.33}$$

and is the temperature at which pairs of infinite separation unbind. Above $T_{\rm KT}$ both $\tilde{\epsilon}$ and y^2 become large, indicating that σ_s^0 is being renormalized to zero and that very large pairs are becoming significantly probable. Note that Eq. (2.33) implies that

$$\sigma_s(T_{\rm KT})=\frac{2km^2}{\pi\hbar^2}T_{\rm KT}\ . \tag{2.34}$$

This is the central result of the static theory. Equation (2.34) predicts a universal jump in superfluid density at the static transition temperature.

C. Linear dynamic theory

Since many experiments are performed at finite frequencies, in which there is an oscillating superfluid flow, it is important to incorporate the static theory of Sec. II B into a more comprehensive theory that accounts for the ac response of the vortex plasma. The motion of vortices is assumed to be diffusive in these systems so that it is intuitively clear that the vortex-diffusion length r_D should play an important role in the dynamics. This length, in fact, determines the crossover between smaller pairs which can equilibrate to the oscillating field and larger pairs which cannot. The theory outlined below, which was developed by Ambegaokar, Halperin, Nelson, and Siggia[5,16] (AHNS), relates r_D to the response of the superfluid in terms of a complex dynamical dielectric constant ϵ defined by

$$\mathbf{V}_s(\omega)=[1-\epsilon^{-1}(\omega)]\mathbf{V}_n(\omega)\ , \tag{2.35}$$

where ω is the frequency of oscillation. This generalized dielectric constant is analogous to $\tilde{\epsilon}$ in the static theory and has contributions from both bound pairs and free vorticity.

Ambegaokar and Teitel[4] derived the response function of a test pair in an oscillating field and extracted the corresponding contribution to the dielectric constant. They considered the equivalent problem of the diffusive motion of charged rods in an oscillating electric field. The motion of the rods is governed by the Langevin equation,

$$\frac{d\mathbf{r}}{dt}=\frac{-2D}{kT}\frac{\partial U}{\partial \mathbf{r}}+\boldsymbol{\eta}(t)\ , \tag{2.36}$$

where $\mathbf{r}$ is the vector along the length of the rod, D is the rod diffusivity, U is the potential energy of the rod, and $\boldsymbol{\eta}$ is a Gaussian noise source satisfying

$$\langle \eta^{\alpha}(t)\eta^{\beta}(t')\rangle=4D\delta_{\alpha\beta}\delta(t-t')\ . \tag{2.37}$$

This last relation is a statement of the dissipation-fluctuation theorem and is discussed in Sec. II E. The potential U is

$$U(r)=2q^2\int_{r_0}^{r}\frac{dr'}{r'\tilde{\epsilon}(r')}-q\delta\mathbf{E}\cdot\mathbf{r}-2u_0\ , \tag{2.38}$$

where $2u_0$ is the chemical potential for the creation of a rod and $\delta\mathbf{E}$ is a small external (oscillating) electric field. Again, the vortex language is recovered using Eq. (2.18).

The response function is a solution to the Fokker-Planck equation, which is obtained from Eq. (2.36)

$$\frac{d\delta n(r,t)}{dt}=\frac{2D}{kT}\frac{\partial}{\partial\mathbf{r}}\cdot\left[\frac{\partial U}{\partial\mathbf{r}}\delta n(r,t)\right]+2D\frac{\partial^2\delta n(r,t)}{\partial r^2}\ , \tag{2.39}$$

where $\delta n(r,t)$ is the density of pairs per unit area of separation. Ambegaokar and Tietel solved this equation to first order in $\delta\mathbf{E}$. They then used the resulting expression for $\delta n(r,t)$ to calculate ϵ_b—the bound pair contribution to ϵ. In general,

$$\epsilon_b(\omega)=1+2\pi q\int d^2r\,\mathbf{r}\cdot\frac{\partial\delta n}{\partial\mathbf{E}} \tag{2.40}$$

which when combined with the solution of Eq. (2.39) becomes

$$\epsilon_b(\omega)=1+\int_{r_0}^{\infty}dr\left[\frac{d\tilde{\epsilon}}{dr}\right]g(r,\omega)\ , \tag{2.41}$$

where $g(r,\omega)$ is a complex pair response function approximated by

$$g(r,w)\approx\frac{14D}{14D-ir^2\omega} \tag{2.42}$$

and $d\tilde{\epsilon}/dr$ is determined from the recursion relations of Sec. II B. The response function varies rapidly compared to $d\tilde{\epsilon}/dr$ so that the former may be approximated by

$$\mathrm{Re}[g(r,\omega)]=\Theta(14D-r^2\omega)$$
$$\mathrm{Im}[g(r,\omega)]=\tfrac{1}{4}\pi r\delta(r-r_D) \tag{2.43}$$

where Θ is a step function defined by

$$\Theta(x)=\begin{cases}1 & \text{for } x>0\ ,\\ 0 & \text{for } x\le 0\ ,\end{cases}$$

and r_D is the diffusion length

$$r_D=\sqrt{14D/\omega}\ . \tag{2.44}$$

Inserting Eqs. (2.43) into (2.41), the resulting expression for ϵ_b in the vortex language is

$$\mathrm{Re}(\epsilon_b)=\tilde{\epsilon}(l_\omega) \tag{2.45}$$

$$\mathrm{Im}(\epsilon_b)=K_0\pi^4y^2(l_\omega)\ , \tag{2.46}$$

where

$$l_\omega = \frac{1}{2}\ln\left[\frac{14D}{\omega r_0^2}\right] . \tag{2.47}$$

Thus the physical interpretation of Eq. (2.45) is that pairs larger than r_D do not contribute to the renormalization of σ_s^0 so that the iteration must be truncated at $l = l_\omega$. Equation (2.46) accounts for pairs with separation of order r_D. These pairs are maximally out of phase with the oscillating field and give rise to dissipation.

Free charge (vorticity) is assumed to diffuse in the macroscopic electric (superfluid) field. This gives rise to an additional imaginary contribution to the dielectric constant

$$\epsilon_f = i4\pi n_f q^2 D/(kT\omega) \tag{2.48}$$

where n_f is the areal density of free charges. In the vortex language

$$\epsilon_f = i4n_f\pi^2 K_0 D/\omega . \tag{2.49}$$

There are two possible sources of free vorticity: that induced from rotation and that arising from pair dissociation. Pair dissociation occurs when pairs are thermally activated over the separation at which they are still bound. Below $T_{\rm KT}$, all pairs are bound (in an infinite system), at least for infinitesimal external fields. Above $T_{\rm KT}$, a correlation length ξ_+ can be defined which represents the length scale at which pairs begin to unbind. The thermally activated free vortex density is believed to be related to ξ_+ by[16]

$$n_f = F/\xi_+^2 , \tag{2.50}$$

where F is a parameter of $O(1)$. In terms of Kosterlitz-Thouless theory, ξ_+ is defined by the value of l at which $y^2(l)$ iterates back to order y_0^2 (see Fig. 7). AHNS have shown that in the temperature domain,

$$\xi_+ \approx r_0 \exp\left[\frac{2\pi}{b\sqrt{t}}\right] , \tag{2.51}$$

where t is the reduced temperature

$$t = T/T_{\rm KT} - 1 \tag{2.52}$$

and b is a nonuniversal parameter. There is no simple physical interpretation of b—it presumably reflects the temperature dependence of the bare superfluid density and vortex fugacity.

D. Finite amplitude effects

The theory outlined in Sec. II C assumes that infinitesimal external fields are used to probe the vortex plasma. In practice this assumption is easily violated—requiring an analysis of nonlinear finite amplitude effects. In the charged plasma formalism, the energy of a pair in an electric field $\mathbf{E}$ is

$$U(r) = 2q^2 \int_{r_0}^{r} \frac{dr'}{r'\tilde{\epsilon}(r')} - q\mathbf{E}\cdot\mathbf{r} - 2u_0 . \tag{2.53}$$

The dipole term in Eq. (2.53) leads to two major modifications of the linear theory. The first is related to the fact that the potential energy $U(r)$ has a saddle point at $r = (r_c, 0)$ where,

$$r_c = \frac{2q}{E\tilde{\epsilon}(r_c)} . \tag{2.54}$$

AHNS have used the 2D Coulomb plasma analyses of McCauley[17] and Huberman *et al.*[18] together with the nucleation theory of Langer and Reppy[19] to calculate the rate R at which pairs nucleate over r_c and dissociate. The calculation begins by obtaining the Fokker-Planck equation given by Eq. (2.39). This is then solved by expanding $U(r)$ in the neighborhood of $(r_c, 0)$

$$\exp(-U/kT) \approx \frac{r_0^4}{r_c^4} y^2(l_c)\exp[2\pi K(l_c)] \times \exp\left[\frac{\pi K(l_c)(\delta x)^2}{r_c^2}\right] \times \exp\left[\frac{-\pi K(l_c)(\delta y)^2}{r_c^2}\right] , \tag{2.55}$$

where

$$l_c = \ln(r_c/r_0) \tag{2.56}$$

and δx and δy are deviations from $(r_c, 0)$. The number of pairs separating across the saddle point, per unit area per unit time, is

$$R = \frac{2D}{r_c^2} y^2(l_c)\exp[2\pi K(l_c)] \tag{2.57}$$

in the vortex formalism.

To determine the steady-state density of free vorticity n_c, resulting from this nucleation process, one must also consider the rate of recombination. The rate of change of n_c is

$$\dot{n}_c = R - V_p \sigma_c n_c^2 , \tag{2.58}$$

where σ_c is the cross section for pair recombination (of order r_c) and V_p is the average vortex velocity perpendicular to the flow. The vortex velocity is obtained from Eq. (2.35)

$$V_p \propto 2\pi K(l_c) D/r_c \tag{2.59}$$

and the steady-state solution to Eq. (2.58) is

$$n_c = \left[\frac{R}{2\pi K(l_c)}\right]^{1/2} . \tag{2.60}$$

The second modification of the linear theory comes in the derivation of the recursion relations outlined in Sec. II B. Clearly, a finite flow field will change the pair distribution—causing pairs to "stretch" and polarize. Therefore, the dipole term in Eq. (2.53) must be included in the Boltzmann factors which arose in the calculation of the plasma polarizability $\alpha(r)$ and separation density $\delta n(r)$. Gillis *et al.*[20] derived a set of modified recursion relations for a vortex pair in a finite (oscillating) superfluid flow field. The energy of such a pair Eq. (2.53) can readily be used in the Boltzmann factors if it is assumed that a

typical pair lifetime is much longer than the oscillation period of V_s so that the dipole term can be averaged over all possible orientations of the pair. The susceptibility is then

$$\chi(r)=\pi^2 K_0 \int_{r_0}^{r} r^2 \langle \delta n(r) \rangle_\theta dr^2 , \tag{2.61}$$

where

$$\langle \delta n(r) \rangle_\theta = \frac{y_0^2}{r_0^2} \exp\left[-2\pi K_0 \int_{r_0}^{r} \frac{dr'}{r'\tilde{\epsilon}(r')} \right] I_0(\Gamma \sigma_s^0 V_s r/kT) \tag{2.62}$$

and I_0 is a zeroth-order modified Bessel function. The modified recursion relations resulting from Eqs. (2.61) and (2.62) are

$$K^{-1}(l)=K_0^{-1}+4\pi^3 \int_0^l y^2(l')dl' \tag{2.63}$$

$$y^2(l)=y_0^2 \exp\left[4l - 2\pi \int_0^l K(l')dl' \right] I_0(2\pi K_0 e^l V_s/V_0) , \tag{2.64}$$

where

$$V_0=\frac{\hbar}{m r_0} . \tag{2.65}$$

Note that the finite-amplitude recursion relations differ from the linear relations only in the I_0 factor in Eq. (2.64) and that setting V_s equal to zero recovers Kosterlitz-Thouless relations.

E. Vortex diffusivity

The diffusivity of a vortex line is defined as

$$D=\tfrac{1}{2} \int_0^\infty \langle \mathbf{V}_L(t)\cdot\mathbf{V}_L(0) \rangle dt , \tag{2.66}$$

where $\mathbf{V}_L(t)$ is its velocity at time t. This equation measures the area swept out per unit time by a randomly walking vortex.

In a 3D system, D is approximately equal to the "bulk" diffusivity determined as follows: Vortices are acted upon by the collective excitations of the fluid (i.e., rotons, ripplons, phonons) and thus provide a coupling mechanism between the superfluid and normal fluid components. Hall and Vinen[21] studied the interaction of a vortex line with the normal fluid and identified a drag force per unit line length of the form,

$$\mathbf{f}_D = B(\mathbf{V}_L-\mathbf{V}_n)+B'\hat{\mathbf{z}}\times(\mathbf{V}_L-\mathbf{V}_n) , \tag{2.67}$$

where $\hat{\mathbf{z}}$ is the unit vector along the core of the line, and B and B' are phenomenological drag coefficients. There is also an interaction between a vortex line and the superfluid (Magnus force),

$$\mathbf{f}_M = \rho_s \Gamma(\mathbf{V}_L-\mathbf{V}_s) , \tag{2.68}$$

where $\Gamma=2\pi\hbar/m$ and ρ_s is the bulk superfluid density. Finally, if the substrate on which the line terminates is "rough" then vortex lines will hydrodynamically "pin" to microscopic protuberances. This produces a static friction-type force of the form[22]

$$\mathbf{f}_b = \begin{cases} -(\mathbf{f}_D+\mathbf{f}_M) & \text{for } |\mathbf{f}_D+\mathbf{f}_M| \le f_p , \\ -f_p \hat{\mathbf{V}}_{Lb} & \text{for } |\mathbf{f}_D+\mathbf{f}_M| > f_p , \end{cases} \tag{2.69}$$

where $\mathbf{V}_b$ is the substrate velocity, $\hat{\mathbf{V}}_{Lb}$ is a unit vector in the direction of $(\mathbf{V}_L-\mathbf{V}_b)$, and f_p is the static pinning force per unit line length, of order

$$f_p \approx \frac{\rho_s \Gamma^2}{4\pi L} ln(b/r_0) , \tag{2.70}$$

where L is the line length and b is the interline spacing. Assuming that a vortex line has negligible inertial mass, the sum of the forces acting on it must balance,[23]

$$\mathbf{f}_b+\mathbf{f}_M+\mathbf{f}_D=\mathbf{0} \tag{2.71}$$

and the line moves with a velocity which satisfies Eq. (2.71). If f_p is neglected (the substrate is smooth) then the solution to Eq. (2.71) is

$$\mathbf{V}_L = \frac{2\pi D_b \hbar \rho_s}{mkT} \hat{\mathbf{z}}\times(\mathbf{V}_n-\mathbf{V}_s)+C(\mathbf{V}_n-\mathbf{V}_s)+\mathbf{V}_s , \tag{2.72}$$

where

$$D_b = kT \frac{B}{(\Gamma\rho_s-B')^2+B^2} \tag{2.73}$$

is the "bulk" diffusivity and

$$C=1-\frac{(\rho_s\Gamma-B')\Gamma\rho_s}{(\Gamma\rho_s-B')^2+B^2} . \tag{2.74}$$

This expression relates D_b to vortex interactions with ripplons, rotons, and phonons through the phenomenological drag parameters B and B'. To be self-consistent, however, the fluctuations in the local superfluid and normal-fluid velocities which actually give rise to diffusive motion, must be included in Eq. (2.72). This is done by adding a small fluctuating velocity term to the right-hand side of the equation, as in the case of Eq. (2.36), whose autocorrelation function is proportional to D, Eq. (2.37). This noise term not only has contributions from rotons, phonons, and ripplons but may also have contributions from surrounding vorticity. Clearly, in two dimensions, where vortex-pair fluctuations become important, a test vortex may experience substantial fluctuations in the local superfluid velocity field as a result of the motion of surrounding pairs.

The importance of understanding the origin and temperature dependence of diffusivity in 2D helium systems is apparent when one realizes that almost all finite frequency experiments performed on the Kosterlitz-Thouless transition have been interpreted via the AHNS theory outlined in Sec. II C. Though D is the primary transport parameter of this theory, its value has for the most part been assumed to be of order $\hbar/m$ in the literature. This value has been argued purely on dimensional grounds by AHNS and misleadingly implies that D is temperature independent.

Diffusivity appears in two ways in the dynamic theory: it comes in logarithmically in the cutoff l_ω to the bound pair contribution to ϵ and it is a prefactor in the free vortex contribution to ϵ. Previous efforts to fit the former to

experimental data have not been very successful because of l_ω's logarithmic dependence on D. The first such effort was that of Bishop and Reppy[24] who used an oscillating substrate to measure the dissipation and superfluid density of thin films of helium as a function of temperature through the transition. Their experiment essentially measured the real and imaginary parts of ϵ, see Sec. III B, to which they compared the predictions of the AHNS theory. They fit their data to an approximate solution of the recursion relations which is valid for small reduced temperatures

$$\begin{aligned} &\mathrm{Re}[\epsilon_b] \propto 1-0.5X(l_\omega) \\ &\mathrm{Im}[\epsilon_b] \propto Y^2(l_\omega) , \end{aligned} \tag{2.75}$$

where

$$\begin{aligned} &X(l_w)\approx 0.5\sqrt{t}\,\coth(0.5b\sqrt{t}\,l_\omega) , \\ &4\pi Y(l_\omega)\approx 0.5b\sqrt{t}\,\operatorname{csch}(0.5b\sqrt{t}\,l_\omega) \quad \text{for } t<0 , \end{aligned} \tag{2.76}$$

and b is the nonuniversal parameter of Sec. II C which absorbs information about $K_0(T)$ and $y_0^2(T)$. [The hyperbolic functions in Eq. (2.76) become sinusoidal for $t>0$.] A typical measurement of the reduced period, which is roughly proportional to the superfluid density, and the excess dissipation of Bishop and Reppy's oscillator is shown in Fig. 1. The solid lines are fits to the data using Eqs. (2.75) and (2.76) for ϵ_b and Eq. (2.50) for the thermal free vortex contribution. The fit uses six parameters: $\sigma_s(T_{\mathrm{KT}})$, b, l_ω, F, T_{KT}, and ϵ' (ϵ' is to account for the anomalous dissipation tail on the cold side of the peak). The fit shown in Fig. 1 is for $l_\omega=12$ which corresponds to $D\approx 20\hbar/m$. This is roughly an order of magnitude larger than conjectured by AHNS.

Diffusivity has also been extracted from thermal conductivity data in a manner similar to Bishop and Reppy's approach. Agnolet *et al.*[25] have measured the thermal conductance of helium films in conjunction with torsional oscillator measurements of the superfluid density. The film conductance as given by the AHNS theory is

$$K_{\mathrm{film}}=\frac{m\chi S_g kT}{2\pi\hbar D n_f} , \tag{2.77}$$

where S_g is the entropy per unit mass of the vapor above the film, L is the latent heat of evaporation per unit mass, χ is a cell geometrical factor, and n_f is the density of thermally activated free vortices. Inserting the expression for n_f, Eq. (2.51), into Eq. (2.75)

$$K_{\mathrm{film}}=\frac{m\chi L S_g kT}{2\pi\hbar D} r_0^2 \exp\left[\frac{4\pi}{b\sqrt{t}}\right] . \tag{2.78}$$

Agnolet *et al.* used the torsional oscillator data to determine T_{KT} and then plotted $\ln(K_{\mathrm{film}})$ versus $\sqrt{t}$ from their conductance data, see Fig. 2. From the slope and intercept of the plots they were able to extract b and D/r_0^2. They reported $D/r_0^2\approx 6\times 10^{-11}$ sec^{-1} for $T_{\mathrm{KT}}\approx 1.28$ K which corresponds to $D\approx 0.8\hbar/m$.

Finotello and Gasparini[26] have also extracted b and D/r_0^2 from conductance measurements in thin films of helium. They used essentially the same method as Agnolet *et al.* (without the oscillator) and reported $D/r_0^2\approx 5\times 10^{-12}$ sec^{-1} for T_{KT} in the range 1.4–1.9 K. This corresponds to $D\approx 0.1\hbar/m$.

Implicitly implied in the analyses of the experiments discussed above, is that D is independent of temperature near the transition. There is no reason to believe that this is so, and Kim and Glaberson[27] have, in fact, provided firm experimental evidence for a strongly temperature-dependent diffusivity in the region near the transition. They measured the effect of a known density of rotation-induced free vorticity n_Ω on a high-Q third-sound resonant cavity. They observed a damping of the third-sound resonance which they associated with the diffusive motion of the induced vorticity. Using the AHNS third-sound analyses, it is easy to show that D is proportional to the

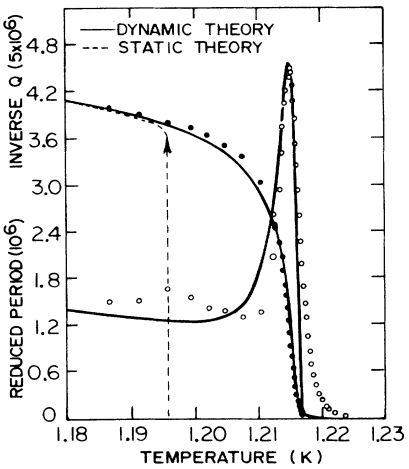

FIG. 1. Data from Ref. 18. The reduced period and excess dissipation for superfluid transition at 1.215 K. The solid lines are fits using the dynamic theory of AHNS. The dashed line is the static theory prediction.

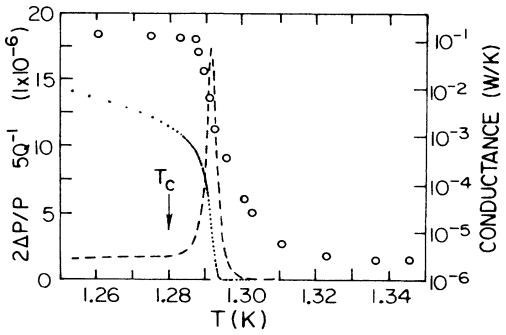

FIG. 2. Data from Ref. 19. The reduced period and dissipation of the torsional oscillator are shown along with the total cell conductance (open circles). The T_c indicated is T_{KT} in the present notation.

excess full width resonance induced by rotation, $\Delta\omega$,

$$D=\frac{kT\Delta\omega}{4\pi^2(\hbar/m)^2 n_\Omega \sigma_s}\ , \tag{2.79}$$

where n_Ω is given by the expression

$$n_\Omega = m\Omega/\pi\hbar\ , \tag{2.80}$$

and Ω is the rotation angular velocity. Kim and Glaberson characterized their data by

$$D\approx 0.17\left[\frac{\hbar}{m}\right]\left[\frac{kT}{\sigma_s}\right]^2 \tag{2.81}$$

and reported $D\approx 0.4\hbar/m$ at $T=T_{KT}$. Equation (2.81) is a rapidly increasing function of T near T_{KT} in that σ_s is renormalized to zero in that region. This observed rapid variation in D near T_{KT} may explain the wide discrepancy in diffusivities reported in other experiments which do not directly measure it.

III. EXPERIMENTAL METHOD

A. Oscillating substrate method

We have utilized the oscillating substrate method of Bishop and Reppy[24] in which we monitor the period and amplitude of a high-Q torsional oscillator, containing a small amount of ^{4}He, as the temperature is swept through the Kosterlitz-Thouless transition. This method is a variation of Andronikashvili's[28] technique for measuring the superfluid density in bulk ^{4}He. The original Andronikashvili experiment made use of a stack of closely spaced disks which were attached to a torsion fiber so as to form a torsional oscillator. The disks were placed in a helium bath and the resonant frequency was monitored as a function of temperature. The disk spacing was chosen to be much smaller than the viscous penetration depth of the normal fluid, thus clamping the normal component to the oscillator. Since the superfluid component did not couple to the oscillator, the effective moment of inertia of the latter was a direct measure of ρ_s.

The present method of using a high-Q torsional oscillator with a resonant frequency of 500 Hz has two advantages over the relatively low-Q–low-frequency method of Andronikashvili. First, because there is little damping in the torsion member, the amplitude of the oscillator is very sensitive to changes in the internal dissipation of the superfluid. Second, with this method one is able to achieve very stable resonant frequencies—in our case, we were able to measure period changes on the order of one part in 10^9. This corresponds to a sensitivity to less than one hundreth of one layer of helium on the substrate.

The experimental apparatus is shown in Fig. 3. The oscillator and isolation masses were contained in a vacuum can surrounded by a helium bath. The oscillator itself consisted of four main parts: the experimental cell into which helium films were deposited, a high-Q Be-Cu torsion rod, a set of capacitive pickups which detected the oscillatory motion of the cell, and a magnetic drive. The cell was made of magnesium and was approximately 2.5-cm high and 2.5 cm in diameter. It contained a stack of

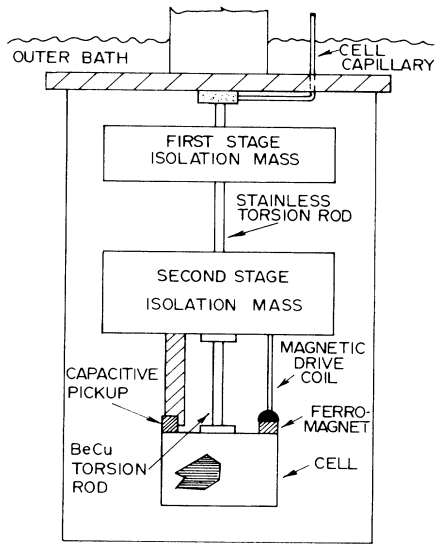

FIG. 3. Diagram of the oscillator and isolation system. For clarity, only one detector is shown.

approximately 9100 0.1-mil Mylar disks which formed the substrate. The disks were simply "pressed" into the cylindrical cell which left about a 1200-Å spacing between them and a 1-cm^3 dead space in the stack assembly. To ensure that the helium would make its way through the entire stack, a small pin hole was punched in the center of each disk before being placed in the cell. The effective substrate area of this arrangement was about 8.0×10^4 cm^2. Helium was introduced into the cell through a 1/8-in. hole that ran up through the Be-Cu rod and the two isolation masses to a capillary at the top of the vacuum can.

The Be-Cu torsion rod was machined before annealing it at 650 F for 2 h. This annealing process hardened the rod so as to minimize hysteretic losses in the oscillator. The rod was machined with flanges on either end and was connected to the cell and the lower isolation mass with machine screws and indium o rings.

Two 2-cm-high and 1-cm-wide fins were machined out of the top of the cell as part of the capacitive detector system. The fins were located opposite to one another with their edges lying on the same diameter. The other half of the two pick-up capacitors were attached to an epoxy jig on the bottom side of the lower isolation mass. The pick-up capacitors were connected in parallel and were carefully adjusted so as to eliminate sensitivity to transverse "bending" modes of oscillation. The average plate separation was $d_0\approx 2.5\times 10^{-2}$ cm and the effective capacitive area was $A_c\approx 2.0$ cm^2.

The oscillator was driven by a superconducting coil, attached to the lower isolation mass, which interacted with a small samarium-cobalt ferromagnet epoxied to the top of the cell. The drive coil was carefully shielded to prevent crosstalk with the detectors. Typical drive currents were tenths of a milliamp.

The cell was set into oscillation by a positive-feedback arrangement that consisted of the detectors, the magnetic

drive, and a constant current feedback circuit. The dC_p/dt signal from the detectors was fed to a current to voltage converter with gain of 10^9 V/A. The resulting amplified signal was then fed to the feedback circuit shown in Fig. 4 which in turn supplied the superconducting drive coil. The drive circuit consisted of a phase shifter, a zero-crossing detector, and a constant-current source. The phase shifter was adjusted to positively feed back the signal to the drive coil. This caused the system to spontaneously oscillate at its resonant frequency (determined by the cell and the torsion member) much in the same way a public address system will "screech" if the microphone is held too close to the speaker. The zero-crossing detector and constant-current-output stage were designed to allow the drive to be independent of the amplitude of oscillation.

The two upper isolation masses along with their stainless-steel torsion members formed a second-order mechanical filter. This system isolated the oscillator from the cryostat which served two functions. First, mechanical vibrations from the cryostat, which were substantial during rotation, were greatly reduced thereby improving our signal to noise ratio. Second, the isolation system helped to reduce energy losses arising from vibrational coupling to the cryostat. At low temperatures, where hysteretic losses in the Be-Cu rod are small, this coupling becomes important and can limit the Q of the oscillator.

B. Response of oscillator and measurement of D

The oscillator system described in Sec. III A was used to determine the effective mass (i.e., the superfluid density) and dissipation of thin films of ^{4}He as a function of temperature. To simplify the analysis of its response we can work in "linear" units by dividing the moment of inertia and torsion constant by $\frac{1}{2}R_{\text{cell}}^2$, where R_{cell} is the cell radius. At resonance, the amplitude of oscillation is

$$A=\frac{f_0 Q}{k_0}\ , \tag{3.1}$$

where f_0 is the driving force determined by the setting of the drive circuit output, k_0 is the effective spring constant, and Q is the quality factor of the oscillator. For constant f_0 and constant external damping,

$$\Delta A^{-1}\propto \Delta Q^{-1}\ , \tag{3.2}$$

where ΔQ^{-1} represents changes in the superfluid dissipation. The films we will be considering are quite thin (a few layers of atoms) compared with the normal-fluid viscous penetration depth and the normal component is always clamped to the substrate.

The period of oscillation is related to its total effective mass, M (including the film) by

$$P=2\pi\left[\frac{M}{k_0}\right]^{1/2}\ . \tag{3.3}$$

Because the superfluid does not couple to the substrate, we can write M as

$$M=M_0-M_s\ , \tag{3.4}$$

where M_0 is the mass of the cell, the substrate, and the normal fluid and M_s is the superfluid mass. M_s is related to σ_s by

$$M_s=\sigma_s A_s\ , \tag{3.5}$$

where A_s is the substrate area. Assuming $M_0\gg M_s$, the period of the oscillator is

$$P=P_0\left[1-\frac{1}{2}\frac{\sigma_s A_s}{M_0}\right]\ . \tag{3.6}$$

Dropping the P_0 and M_0 notation,

$$\frac{2\Delta P}{P}=\frac{\sigma_s A_s}{M}\ , \tag{3.7}$$

where ΔP is relative to P. The area to mass ratio in Eq. (3.7) determines the sensitivity of the system. This quantity was determined by first attaching known masses to the oscillator and measuring the resulting changes in the period to determine its effective mass, $M=56$ g, and spring constant, $k_0=5\times10^8$ erg/cm. The area of the substrate was taken to be the geometrical area of the Mylar disks, $A_s=8.0\times10^4$ cm^2 and $A_s/M=1430$ cm^2/g.

Equations (3.2) and (3.7) relate changes in the amplitude and period of the oscillator to changes in the dissipation and density of the superfluid film. To make use of the dynamic theory of Sec. II B one must express the response of the oscillator in terms of the complex dielectric constant ϵ, defined by Eq. (2.35). The momentum density of the film is simply

$$\mathbf{g}=\sigma_s^0\mathbf{V}_s(t)+(\sigma-\sigma_s^0)\mathbf{V}_n(t)\ , \tag{3.8}$$

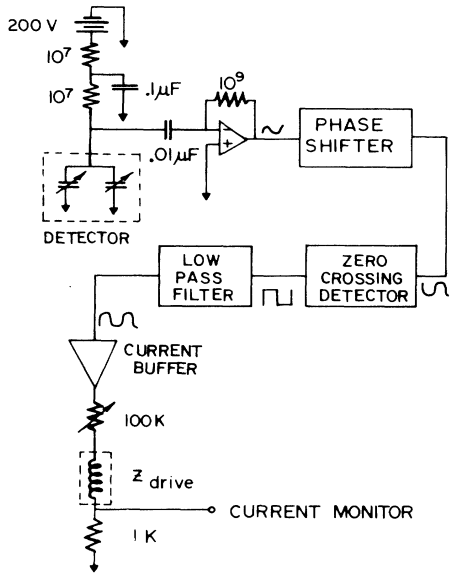

FIG. 4. Schematic of the detector and positive feedback circuit. The dashed lines indicate components attached to the oscillator.

where σ is the areal mass density of helium and

$$\mathbf{V}_s(t)=\mathbf{V}_s e^{-i\omega t}, \quad \mathbf{V}_n(t)=\mathbf{V}_n e^{-i\omega t} . \tag{3.9}$$

Using Eq. (2.35), we can write the reaction force on the substrate as

$$\mathbf{F}(t)=\frac{d\mathbf{g}}{dt}A_s = iA_s\omega[\sigma\mathbf{V}_n(t)-\sigma_s^0\epsilon^{-1}\mathbf{V}_n(t)] . \tag{3.10}$$

The average energy dissipated in one cycle is

$$\Delta E=-P\langle \mathrm{Re}[\mathbf{F}(t)\cdot\mathbf{V}_n(t)]\rangle \tag{3.11}$$

and the corresponding change in Q^{-1} is the ratio of ΔE to the energy stored, $E=\frac{1}{2}MV_n^2$,

$$\Delta Q^{-1}=\frac{\Delta E}{2\pi E}=\frac{A_s\sigma_s^0}{M}\mathrm{Im}(-\epsilon^{-1}) . \tag{3.12}$$

The reaction force of Eq. (3.10) also produces a period shift

$$\frac{2\Delta P}{P}=\frac{A_s\sigma_s^0}{M}\mathrm{Re}(\epsilon^{-1}) . \tag{3.13}$$

In practice we measure the reduced period $2\Delta P/P$ and excess dissipation ΔQ^{-1} of the oscillator as a function of temperature. By inverting Eqs. (3.12) and (3.13) we can then extract ϵ as a function of temperature

$$\mathrm{Re}(\epsilon)=\frac{A_s\sigma_s^0}{M}\frac{\frac{2\Delta P}{P}}{(2\Delta P/P)^2+(\Delta Q^{-1})^2} , \tag{3.14}$$

$$\mathrm{Im}(\epsilon)=\frac{A_s\sigma_s^0}{M}\frac{\Delta Q^{-1}}{(2\Delta P/P)^2+(\Delta Q^{-1})^2} . \tag{3.15}$$

The vortex diffusivity D is determined by measuring the contribution of a known free vortex density n_Ω to $\mathrm{Im}(\epsilon)$. This is done by first measuring $\mathrm{Im}(\epsilon)$ as a function of temperature with the cell at rest and then repeating the measurement with the cell rotating at a frequency Ω. As discussed in Sec. II A, rotation induces a free vortex density which is proportional to the rate of rotation Eq. (2.80). According to Eq. (2.49) the difference between these rotating and nonrotating measurements of $\mathrm{Im}(\epsilon)$ is proportional to D

$$D=[\mathrm{Im}(\epsilon)_\Omega-\mathrm{Im}(\epsilon)_0]\frac{\hbar\omega}{4\pi mK_0\Omega} . \tag{3.16}$$

C. Experimental procedure

Shown in Fig. 5 is a schematic diagram of our experimental system. It consists of four main parts: (1) oscillator and feedback circuit, (2) outer bath thermometry and regulation system, (3) cell thermometry, and (4) computer data aquisition system. The entire cryostat along with low-level amplifiers were rotated on top of a servomotor driven turntable capable of rotation speeds of up to 12 rad/sec. It was necessary to amplify small signals before sending them off the table in order that they be well above the typical 1 mV slip ring noise.

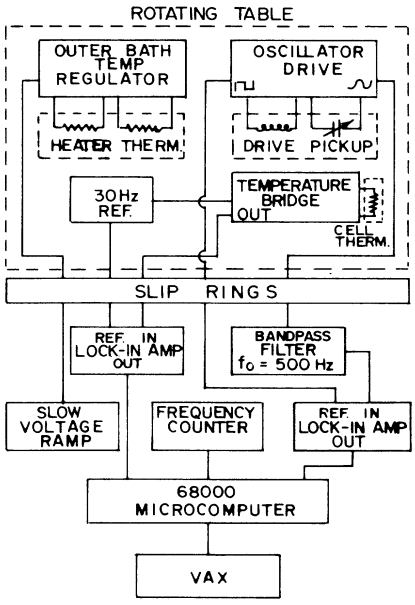

FIG. 5. Block diagram of the electronic instrumentation.

The experimental procedure began by first regulating the outer bath at $T=2.15$ K and then introducing approximately 100 μm of helium gas into the vacuum can. This was done to facilitate the thermal contact with the outer bath and had virtually no effect on the Q of the oscillator. Helium was then transferred into the cell as the period of the oscillator was monitored. The thickness of the film h was obtained from the period change using the equation

$$\frac{2\Delta P}{P}=\frac{\rho h A_s}{M} . \tag{3.17}$$

After transferring helium to the cell the system was allowed to anneal at 1.25 K for approximately 20 min. This was done to ensure that the helium had completely condensed onto the substrate and had saturated the stack. The temperature was then swept up as the period was monitored in order to roughly locate the transition. After finding it, a temperature scale of order 100 mK was calibrated to span the transition and the outer bath was regulated a few millidegrees above T_c. The oscillator was then allowed to ring-down and an exponential was fit to decay of its amplitude (see Fig. 9). The characteristic decay time τ was a direct measure of the background dissipation,

$$Q_0^{-1}=\frac{P}{\pi\tau} \tag{3.18}$$

and was used to calibrate changes in the amplitude of the oscillator to changes in the internal damping. Typical values of Q_0^{-1} were 5.5×10^{-6} to 6.5×10^{-6} depending on the temperature at which the data was taken and the amount of gas in the 1-cm^3 dead space of the cell. After

calibrating the thermometry and the Q^{-1} of the oscillator, its period and amplitude were measured as the outer bath temperature was slowly swept across the appropriate range. A typical temperature scan took 4 h to complete and each data point was averaged over 96 sec. The measurements of the period and Q were relative to their respective values ~ 10 mK above T_c. This corresponded to measuring $2\Delta P/P$ and ΔQ^{-1}. These measurements were first performed with the cell (i.e., the table) at rest and were then repeated with the cell rotating.

IV. NONROTATING DATA

A. Kosterlitz-Thouless transition

Shown in Fig. 6 are the reduced period and excess dissipation of the oscillator for a typical nonrotation transition. These are essentially the results of Bishop and Reppy.[14] The reduced period is roughly proportional to the superfluid density and qualitatively displays Kosterlitz-Thouless behavior. Note the rapid fall in superfluid density at the dynamic transition temperature T_c. Though the superfluid "jump" is rounded from finite frequency effects, its magnitude agrees well with the prediction of Eq. (2.34). The static transition temperature T_{KT} is also displayed on the plot and represents the temperature at which the transition would have occurred at zero frequency. The nonzero superfluid density above T_{KT} is a consequence of the fact that large pairs cannot participate in the renormalization of σ_s^0. The large dissipation peak at T_c is due in part to pairs with separation of order r_D and in part to free vorticity from pair dissociation. As shown in Fig. 6, we did not observe the anomalous dissipation tail reported by Bishop and Reppy (see Fig. 1). This may be associated with the difference between our cell geometries. They used a coiled Mylar substrate in which the substrate normal was perpendicular to the axis of oscillation, whereas, our substrate normal was oriented along the axis of oscillation (and rotation). Bishop[29] has indicated that the excess dissipation tail was observed to be cell dependent and probably was not an inherently interesting property of the system.

B. Fits to the data

We have numerically integrated the recursion relations of Eqs. (2.27) from a locus of initial conditions

$$K_0=\pi\left[\frac{\hbar}{m}\right]^2\frac{\sigma_s^0(T)}{kT}\ , \tag{4.1}$$

$$y_0^2=y_c^2\exp(-CK_0)\ , \tag{4.2}$$

where y_c^2 and C were varied to fit our data. The background superfluid density $\sigma_s^0(T)$ was determined by first measuring $2\Delta P/P$ during the transfer of helium to the cell to determine the total thickness of the film h_T. The effective or dynamic film thickness is h_T minus the thickness of the "dead layer" trapped by the van der Waals attraction to the substrate h_{DL}. In principle the dead layer can be determined by first measuring P at $T=0$ and then repeating the measurement with a known amount of helium in the cell. This assumes, of course, that h_{DL} is a weak function of temperature. The lowest temperature accessible to our system was 1.2 K so that we were only able to make a reasonable estimate of h_{DL}. We took $h_{DL}=10.2$ Å for all of our data and the background superfluid density as

$$\sigma_s^0(T)=(h_T-h_{DL})\rho_s(T)\ , \tag{4.3}$$

where $\rho_s(T)$ carries its temperature dependence.[30] The form of the vortex pair excitation probability, Eq. (4.2), was chosen to be analogous to the form taken by Fiory *et al.*[31] for a Ginsburg-Landau superconductor, where the parameter C is a measure of the vortex core energy.

A schematic of the solutions to Eqs. (2.27) is shown in Fig. 7. The initial conditions are labeled by $l=0$ and the diffusive cutoff by the dashed $l=l_\omega$ curve. Note that above T_{KT}, which corresponds to $K^{-1}/\pi=0.5$, y begins

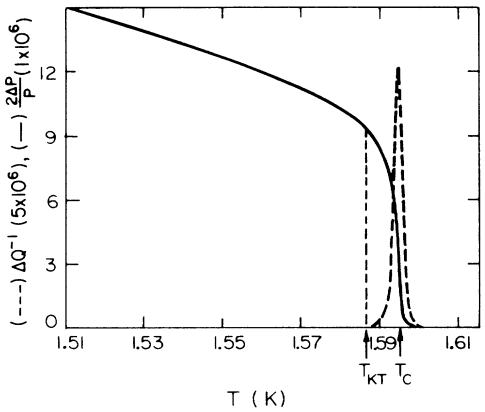

FIG. 6. The reduced period (solid lines) and excess dissipation (dashed line) for a 14-Å film. The arrows indicate the location of the static T_{KT} and dynamic T_c transition temperatures.

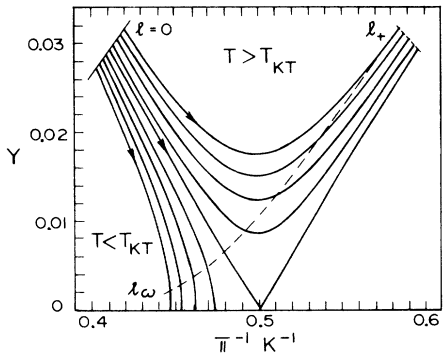

FIG. 7. A schematic of the solutions to the Kosterlitz-Thouless recursion relations. The $l=0$ line represents the initial conditions and the $l=l_\omega$ line represents the diffusive cutoff. The l_+ line is determined by $y(l_+)=y(l=0)$ and defines $\xi_+=r_0\exp l_+$.

to get large. As discussed in Sec. II C the iterations were truncated in this region at the values of l for which $y^2(l) \approx y_0^2$. This defined the two dimensional correlation length which is related to the density of thermally activated free vorticity by Eq. (2.50).

The recursion relations straightforwardly give the real and imaginary bound pair contributions to ϵ for $T < T_{KT}$. Just above T_{KT}, however, free vortex contributions begin to dominate as more and more pairs dissociate. In order to obtain adequate fits to the data, the density of these broken pairs must be estimated. As outlined in Sec. II C, $y^2(l_\omega)$ measures the number of pairs with separation r_D. It is reasonable to assume that $y^2(l_\omega)$ is also a rough measure of the number of pairs with separation substantially larger than r_D—which cannot equilibrate to the field. Though these large pairs are bound, they are dynamically similar to free vorticity. Therefore, we have taken the thermal free vortex density, at all temperatures, to be

$$n_f = \frac{y^2(l_m)}{r_0^2 \exp(2l_m)} , \tag{4.4}$$

where

$$l_m = \begin{cases} l_\omega & \text{for } y^2(l_\omega) \le y_0^2 , \\ l_+ & \text{for } y^2(l_\omega) > y_0^2 . \end{cases} \tag{4.5}$$

Once $K^{-1}(l)$ and $y^2(l)$ were determined, Eqs. (2.45), (2.46), and (2.49) were used to evaluate $\mathrm{Re}(\epsilon)$ and $\mathrm{Im}(\epsilon)$. The theoretical response of the oscillator was then obtained using Eqs. (3.12) and (3.13). The result of a fit to the transition in Fig. 6 is shown in Fig. 8. The relevant parameters used in the fit are the following: $h = 14.0$ Å, $D = 2\hbar/m$, $C = 0.46$, $r_0 = 1.5$ Å, and $y_c^2 = 0.40$. Note that a constant diffusivity was used despite the fact that the present paper reports temperature-dependent diffusivities in Sec. V. This was done for the sake of simplicity since the (nonrotating) fits are relatively insensitive to D. The long-dashed curves in Fig. 8 represent the theory and agree quite well with the data. The short dashed curve represents the predicted reduced period using a temperature-independent background superfluid density $\sigma_s^0(T = 1.585)$. Clearly, the temperature dependence of σ_s^0 is not negligible—even at this relatively low temperature.

It was hoped that the microscopic parameters y_c^2 and C would be temperature independent so that all of our data could be fit by simply making small variations in the measured film thickness. This was not the case, however, as indicated by the parameters obtained in the fit to the transition shown in Fig. 9: $h = 44.2$ Å, $D = 2\hbar/m$, $C = 0.08$, $r_0 = 1.5$ Å, and $y_c^2 = 0.07$. This film is roughly three times thicker than the one in Fig. 8 and required substantially lower values of y_c^2 and C. A possible explanation for the discrepancy in the parameters is that we may have been naive in assuming that $\sigma_s^0 = h\rho_s(T)$ for relatively thin films. The fluctuation spectrum of these films may be significantly different from that of the bulk superfluid. It is also possible, of course, that the microscopic parameters are indeed temperature dependent. Including the effect of reasonable temperature-dependent healing lengths[15] on h_{DL} does not qualitatively affect these conclusions.

As a final note, the short-dashed line in Fig. 9 demonstrates the role of the temperature dependence of $\sigma_s^0(T)$ in sharpening the transition in thicker films. Close to T_λ, $\sigma_s^0(T)$ becomes a strongly decreasing function of temperature and the renormalization occurs over a relatively short-temperature span. The approximate "near-fixed-point" solutions listed in Sec. II E account for this effect with the temperature dependent parameter b at the expense of losing physical insight into its origin.

C. Finite amplitude effects

The transition displayed in Figs. 8 and 9 were well within the linear regime. This was verified by doubling the amplitude of oscillation and rescanning the transitions. This resulted in a negligible change in $2\Delta P/p$ and ΔQ^{-1}. To test the theory of Sec. II D, the superfluid

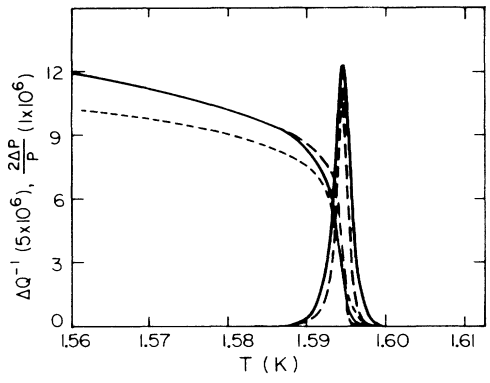

FIG. 8. The reduced period and excess dissipation of a 14-Å film (solid lines). The long dashed lines are fits using the AHNS theory with $y_c^2 = 0.40$ and $C = 0.46$. The short dashed line is a fit using a temperature-independent background superfluid density.

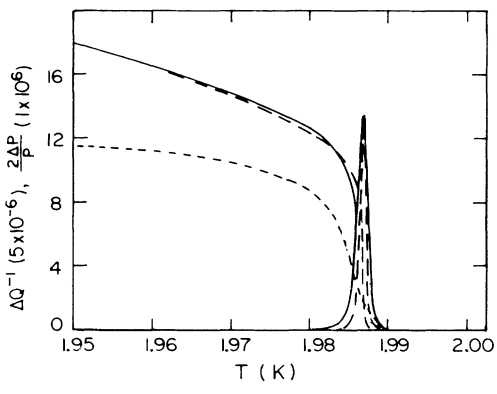

FIG. 9. The reduced period and excess dissipation of a 44-Å film (solid lines). The long dashed lines are fits using the AHNS theory with $y_c^2 = 0.07$ and $C = 0.08$. The short dashed line is a fit using a temperature-independent background superfluid density.

density and dissipation of a film was measured as a function of oscillator drive. Unfortunately, the measurements in this part of the experiment were complicated by the nonlinear response of the oscillator itself at large amplitudes. The raw data had to be "linearized" by first measuring the amplitude and period as a function of drive current i_d (the torque of the drive was assumed to be proportional to i_d) and then fitting the deviations from linear behavior to polynomials. The film's contribution to the reduced period was easily extracted by monitoring the amplitude of the oscillator and factoring out the nonlinear part via the polynomial fit. The excess dissipation of the film was more difficult to extract. It was done by assuming that at resonance, fractional changes in internal damping were equivalent to fractional changes in the drive current—the effect of which we had previously calibrated. An iterative procedure was used to calculate the damping necessary to bring the oscillator amplitude down to the observed levels at a given drive current.

Shown in Figs. 10 and 11 are the linearized reduced period and excess dissipation for the film of Fig. 8. The period was relatively insensitive to the drive current except at the highest values at which there was some rounding. The dominant effect was a systematic widening of the cold side of the dissipation peak. These effects are attributed to pair stretching and pair breaking as a result of large superfluid flows.

The nonlinear theory was tested by applying the modified recursion relations, Eqs. (2.63) and (2.64), to our data. The values of y_c^2 and C obtained from the fit in Fig. 8 were assumed to be amplitude independent and were used in the numerical integration of the equations. The effects of pair breaking were taken into account by including the steady-state pair dissociation density of Eq. (2.60) into the calculation of n_f and by truncating of the iteration at the smallest of the two relevant length scales; l_ω and $l_c = \ln(r_c/r_0)$, where,

$$r_c = \frac{2\pi\hbar}{m\,|V_s|} \,. \tag{4.6}$$

The only adjustable parameter in the fits was the average superfluid velocity V_s used in Eqs. (2.63) and (2.57).

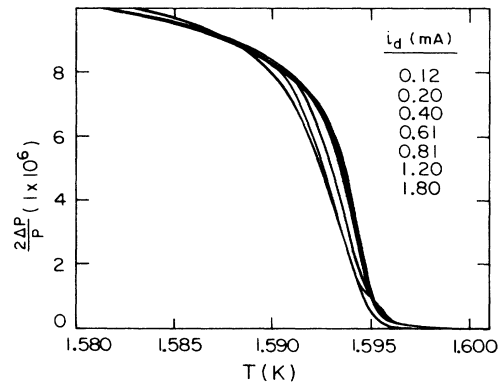

FIG. 10. The reduced period of a 14-Å film for various values of the oscillator drive current i_d.

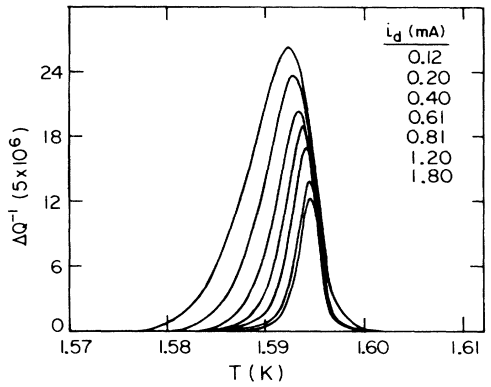

FIG. 11. The excess dissipation of a 14-Å film for various values of the oscillator drive current i_d.

We did not measure the nominal capacitance of the detectors C_p so that we were unable to precisely calibrate the substrate velocity V_b in terms of the detector output voltage V_m. We were, however, able to obtain a reasonable fit to our data by assuming $V_b = \beta V_m$, where β is an adjustable calibration parameter and using Eq. (2.35) to determine V_s. The theoretical predictions are shown in Figs. 12 and 13 for $\beta \approx 0.1$ V sec/cm. (This value of β is consistent with the typical 1-V output of the current amplifier.) The theory seemed to work best at modest substrate velocities—the predicted widening of the dissipation peak was somewhat too large at the highest velocities and the theory underestimates the growth in the peak height with increasing V_b. This leads us to believe that the modified recursion relations may be inadequate for very large superfluid flows. This may be related to Maps and Hallock's observation of an apparent saturation in the number density of velocity-induced free vortices as determined from thermal conductance experiments.[32]

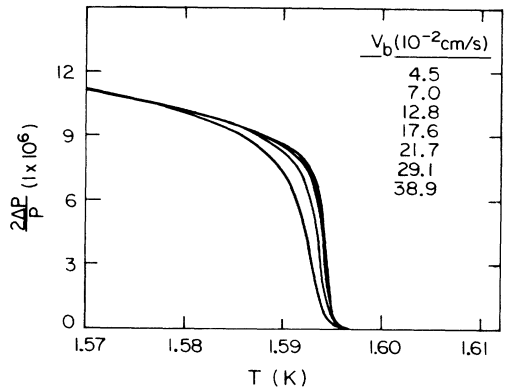

FIG. 12. The prediction of the nonlinear theory for the reduced period of a 14-Å film for various values of the substrate velocity V_b. These curves are to be compared with the data in Fig. 10.

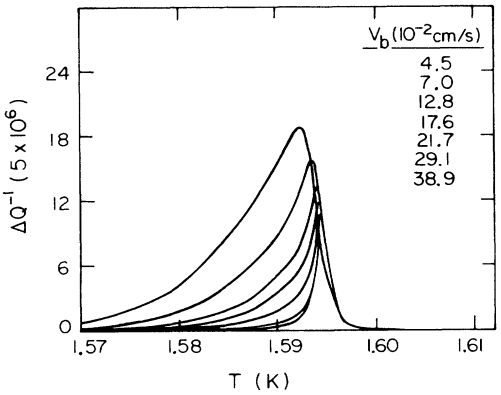

FIG. 13. The prediction of the nonlinear theory for the excess dissipation of a 14-Å film for various values of the substrate velocity V_b. These curves are to be compared with the data in Fig. 11.

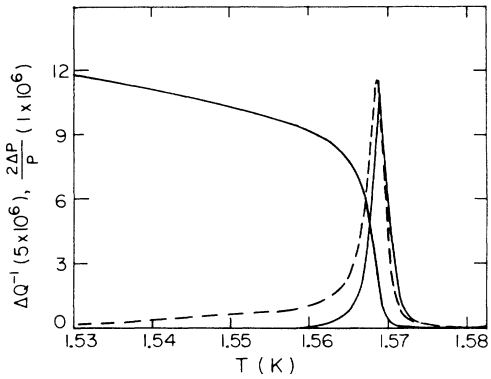

FIG. 15. Solid lines—reduced period and excess dissipation with the cell at rest, for a 11.4-Å film. Dashed lines—reduced period and excess dissipation while rotating at $\Omega=8$ rad/sec.

V. ROTATING DATA AND DIFFUSIVITY

A. Rotating transitions

Shown as solid lines in Figs. 14–16 are the reduced period and excess dissipation for three typical nonrotating transitions. The figures are presented in order of increasing film thickness with the first being one of the thinnest films investigated and the last the thickest. The dashed curves represent the same transitions at a rotation speed of $\Omega=8$ rad/sec ($n_\Omega=1.6\times10^4$ cm^{-2}). Note that in all three films, rotation produced no discernable change in the reduced period. This is expected since n_Ω does not contribute to Re(ϵ). We also did not observe any systematic shift in the transition temperature with rotation. Rotation did cause some small random shifts in temperature which we attributed to the thermometry.

The obvious effect was a rotation induced damping on the cold side of the dissipation peak that grew dramatically as T approached the dynamic transition temperature. This dissipation was observed to extend over 100 mK in the thinner films and less than 30 mK in the thickest. The magnitude of the effect was also observed to be thickness dependent with the largest excess dissipations occurring in the thinnest films. We believe that this excess damping, which was linear in Ω for $T<T_{KT}$, is a direct measure of vortex diffusivity.

B. Measurements of diffusivity

The respective diffusivity measurements for the transitions shown in Figs. 14–16 are displayed in Figs. 17–19 in units of $\hbar/m$. Note that in all three films, D seems to be approaching zero well below T_{KT}, is of order $\hbar/m$ near transition (as conjectured by AHNS) and apparently diverges at T_c. The systematic increase in the sharpness of this behavior with increasing film thickness may be related to the sharpening of the transitions themselves. This trend is clearly demonstrated in Fig. 20 which displays D versus reduced temperature for various film thicknesses.

Note that nothing particularly interesting happens at T_{KT} in the diffusivity plots. One might expect that D would diverge at the static transition temperature since that is the temperature at which very large pairs begin to unbind—possibly causing substantial low-frequency fluc-

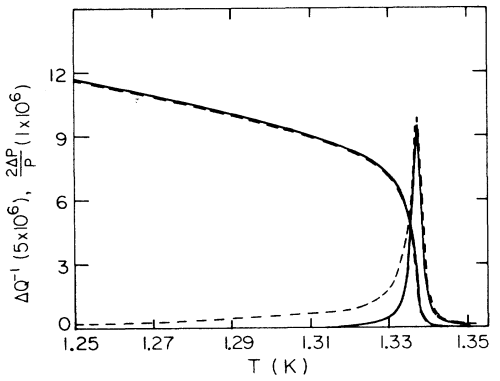

FIG. 14. Solid lines—reduced period and excess dissipation with the cell at rest, for a 6.4-Å film. Dashed lines—reduced period and excess dissipation while rotating at $\Omega=8$ rad/sec.

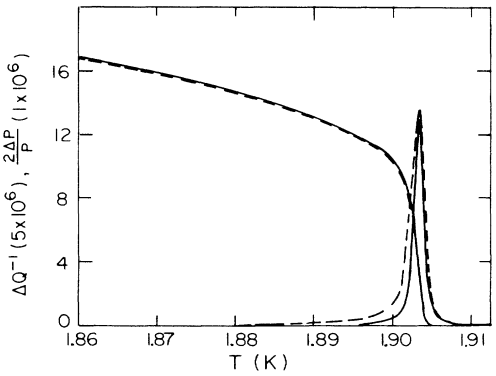

FIG. 16. Solid lines—reduced period and excess dissipation with the cell at rest, for a 30.5-Å film. Dashed lines—reduced period and excess dissipation while rotating at $\Omega=8$ rad/sec.

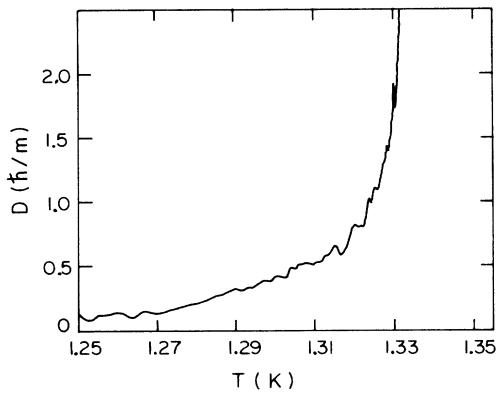

FIG. 17. Diffusivity measurement for the data shown in Fig. 14.

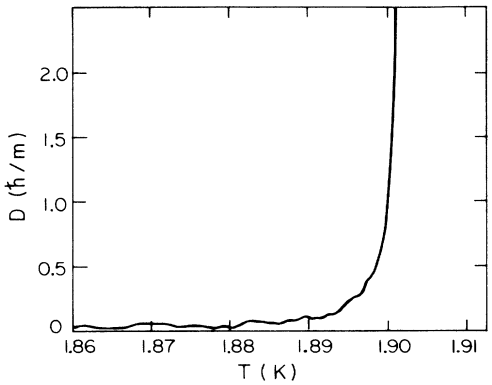

FIG. 19. Diffusivity measurement for the data shown in Fig. 16.

tuations in the local superfluid velocity in the vicinity of a test vortex. We believe that the reason that D remains finite just above T_{KT} is that our system is simply not sensitive to these large scale fluctuations that necessarily occur over many cycles of oscillation. This point is discussed in more detail in the next section.

We have investigated the effect of changing the substrate by predepositing a layer of argon onto the mylar. This was done by transferring 1 atm of argon to the cell at room temperature. There was approximately 1 cm^3 of dead space in the cell and 15 cm^3 in the transfer line on top of the cryostat. Therefore, assuming that almost all of the gas solidified onto the substrate at helium temperatures, a 100-Å film was deposited. The smaller van der Waals attraction of argon (or perhaps smoothing of the substrate associated with the predeposition) resulted in a thinner dead layer and a corresponding increase in T_c for a given film thickness. There was, however, no observed change in either the magnitude or temperature dependence of D as seen in Fig. 21.

We have also investigated the effects of small ^{3}He concentrations on D. A 5% solution of ^{3}He was formed in the cell by monitoring the period change of the oscillator as pure ^{3}He was transferred to a known thickness of ^{4}He. The effect of the ^{3}He was to shift T_c downwards (^{3}He decreases the effective σ_s) but it did not affect D. In fact, within experimental error, the values obtained in the ^{3}He solution were identical to those obtained in pure ^{4}He for a film having the same transition temperature, see Fig. 22.

C. Comparison to other measurements

Figure 23 displays a plot of $D(T_{KT})$ as a function of T_{KT}, where T_{KT} is taken to be the temperature at which our measured σ_s satisifies Eq. (2.34). Though D varies dramatically near the transition $D(T_{KT}) \sim \hbar/m$ in the thinner films and falls to $\sim\frac{1}{2}(\hbar/m)$ in the thickest films (>25 Å).[33] These values should be compared with those of Kim and Glaberson[27] who obtained $D(T_{KT}) \sim 0.4(\hbar/m)$ for 1.3 K $< T_{KT} <$ 1.5 K from third-sound attenuation on a quartz substrate. The temperature dependence of our measurements is in qualitative agreement with that of Kim and Glaberson who reported rapidly increasing diffusivities near the transition. This is discussed in more detail in Sec. V E.

Finotello and Gasparini[26] have also reported $D(T_{KT})$ versus T_{KT} obtained from thermal conductivity measurements on mylar. Their values, however, are roughly an

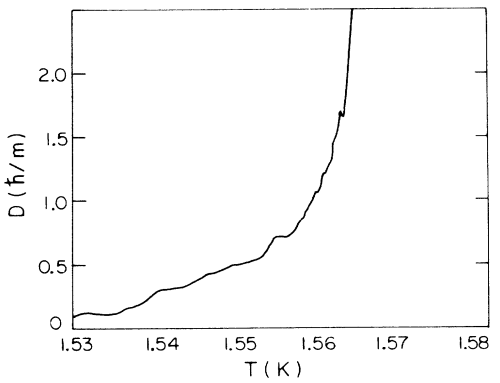

FIG. 18. Diffusivity measurement for the data shown in Fig. 15.

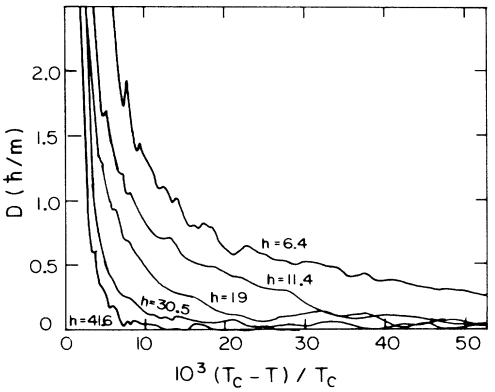

FIG. 20. Diffusivity plotted as a function of reduced temperature for various film thicknesses h (Å).

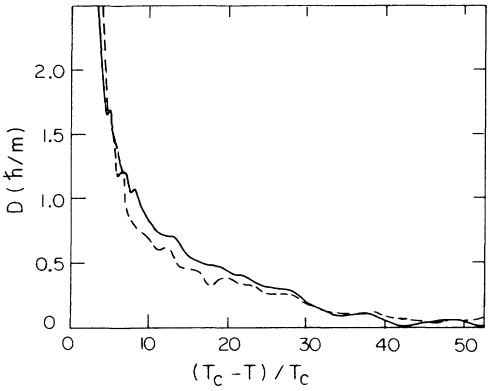

FIG. 21. Solid line—diffusivity measurement for a 10.9-Å film on Mylar. Dashed line—diffusivity measurement for a comparable film on an argon substrate.

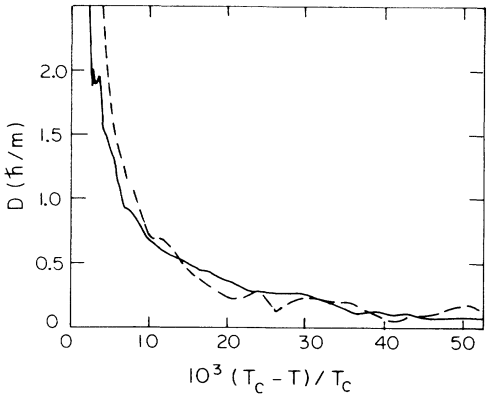

FIG. 22. Solid line—diffusivity measurement for a pure ^{4}He film. Dashed line—diffusivity measurement for a 5% ^{3}He film with a comparable T_c.

order of magnitude smaller than ours and show substantial scatter. This may be a consequence of their experimental method which we believe does not give a reliable measure of diffusivity. The thermal conductance of their films is proportional to $(n_f D)^{-1}$ so that near the transition it is difficult to separate the temperature dependence of n_f from that of D (see Fig. 2). Their crucial assumption that D is independent of temperature in the vicinity of the transition does not appear to be justified.

D. Comparison to theory

There are few theoretical predictions for diffusivity to which we can compare our data. AHNS (Ref. 4) used the definition of D, Eq. (2.66), to show that D is finite at T_{KT}. They failed, however, to address the question as to how D behaves in the region $T_{KT} < T < T_c$. Their analysis is nevertheless enlightening and is outlined below. They assume that the vortex line velocity in Eq. (2.66) is proportional to the local superfluid velocity arising from surrounding pairs. In the dipole approximation, in which only distant pairs are considered,

$$\mathbf{V}_L(t) \propto \int_{R \gg 2r} d^2R \int d^2r\, \delta n(\mathbf{R},\mathbf{r};t)(\mathbf{r}\cdot\nabla)\left[\frac{\mathbf{R}}{R^2}\right], \quad (5.1)$$

where δn is the distribution of vortex pairs with separation $\mathbf{r}$ and location $\mathbf{R}$, relative to the test vortex. To simplify the calculation, AHNS assumed that the effects of the test pair could be ignored. The problem reduces to calculating

$$D \propto \int_0^\infty \int\int\int\int \langle \delta n(\mathbf{R},\mathbf{r};t)\delta n(\mathbf{R}',\mathbf{r}';t')\rangle r_i r_j' d^2r d^2r' d^2R d^2R' dt \quad (5.2)$$

and if the integration over dR' is neglected

$$D \propto \int_0^\infty \int\int \delta_{ij}\delta(\mathbf{R}-\mathbf{R}')\delta n(r) r_i r_j \times \exp(-14Dt/r^2) d^2r\, dR\, dt\ . \quad (5.3)$$

The time dependence in Eq. (5.3) has its origins in the assumed diffusive relaxation of the plasma. AHNS ignored this time dependence and reported

$$D \propto \int_{r_0}^\infty \delta n(r) r^2 dr\ . \quad (5.4)$$

If we make the substitutions

$$\delta n(r) = \frac{y^2(r)}{r^4} \quad (5.5)$$

and $l = \ln(r/r_0)$, then Eq. (5.4) becomes

$$D \propto \int_0^\infty y^2(l) dl\ . \quad (5.6)$$

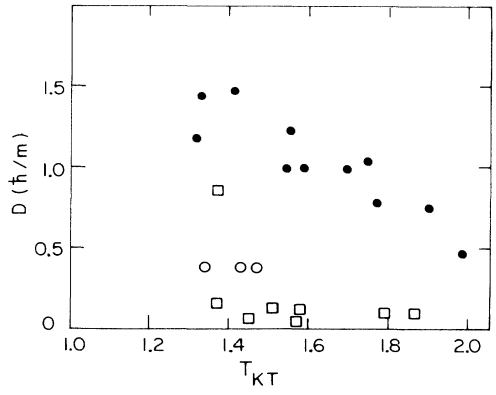

FIG. 23. Diffusivity measured at T_{KT} as a function of T_{KT}. ●—present data, ⊙—Ref. 25, and □—Ref. 24.

This equation can be simplified using Eq. (2.27)

$$D \propto \lim_{l\to\infty} [K^{-1}(l) - K_0^{-1}] \tag{5.7}$$

which is indeed finite at $T = T_{KT}$. This expression grows rapidly as T approaches T_c and predicts $D \propto \bar{\epsilon}$ for large $\bar{\epsilon}$. Though this simple calculation implies that D increases near T_c, its behavior is too sharp when compared with our data ($\bar{\epsilon}$ changes little until $T \sim T_c$).

If the time dependence of Eq. (5.3) is taken into account and the integral from $t = 0$ to ∞ is performed then

$$D \propto \left[\int_0^\infty y^2(l) \exp(2l) dl \right]^{1/2} \tag{5.8}$$

which is divergent since $y^2(l) \propto l^{-2}$ near T_{KT}.[16] This expression can, however, be applied to our data by performing the time integral over one period of oscillation. This is equivalent to neglecting the fluctuations which occur on a time scale large compared to the period. Clearly, our system is not sensitive to vortex motion of wavelength much greater than r_D. We have also only considered contributions from pairs with separation smaller than r_D. This is consistent with the temporal truncation and we have

$$D \propto \int_0^{l_\omega} y^2(l) \exp(2l) \left[1 - \exp\left[\frac{-2\pi r_D^2}{r_0^2 \exp(2l)} \right] \right] dl \ . \tag{5.9}$$

This expression was numerically evaluated using the parameters for the transition in Fig. 8. The resulting curve along with the data is shown in Fig. 24. The predicted variation in D is too rapid near the transition and does not extend down sufficiently far in temperature.

There are also contributions from local pairs and from the movement of the pair centers to the diffusivity which were not included in the calculation of Eq. (5.9). These should be of the same order as dipole contributions and may be important in characterizing D. A more careful calculation, which is beyond the scope of this investigation, is obviously needed.

Huber[34] used the analysis of Taylor and McNamara,[35] which relates the diffusivity of a charge in a 2D plasma to the fluctuations in the electric field, to derive an explicit expression for D. He considered the analogous problem of a 2D charged plasma in a high magnetic field in which the Larmor radius is much less than the Debye length. In this "guiding center" approximation the system is formally equivalent to the $T = 0$ vortex plasma. The equation of motion of a center is

$$\frac{d\mathbf{x}}{dt} = \left[\frac{c}{B^2} \right] \mathbf{B} \times \nabla\phi \tag{5.10}$$

where c is the speed of light, B is the magnetic field, and ϕ is the electrostatic potential. The potential satisfies

$$\nabla^2\phi = 4\pi \sum_j (e_j/l)\delta(\mathbf{r} - \mathbf{x}_j) \ , \tag{5.11}$$

where e/l is the charge per unit length. The energy of two oppositely charged centers is

$$U = \frac{e^2}{l} \ln(r) + \text{const} \ , \tag{5.12}$$

where r is the separation. The vortex formalism is recovered by

$$\begin{aligned} &\frac{-2ce}{lB} \leftrightarrows \hbar/m \ , \\ &\frac{e^2}{l} \leftrightarrows \pi K_0 kT/\bar{\epsilon} \ . \end{aligned} \tag{5.13}$$

The Taylor and McNamara result for the diffusivity of a guiding center plasma in thermal equilibrium is

$$D^2 = \frac{c^2}{4\pi B^2} \int_{k_{\min}}^{k_{\max}} \langle |E(k)|^2 \rangle \frac{dk}{k} \ , \tag{5.14}$$

where $\langle |E(k)|^2 \rangle$ denotes the thermal average of the square of the kth Fourier component of the electric field and $k_{\min}$ and $k_{\max}$ are the spectrum limits. The integrand of Eq. (5.14) can be evaluated using the Debye-Huckle approximation

$$\langle |E(k)|^2 \rangle \approx \frac{4\pi kT}{1 + k\lambda^2} \ , \tag{5.15}$$

where λ is the Debye length. AHNS make the identification

$$n_f = (8\pi\lambda^2)^{-1} = (2\pi\xi_+^2)^{-1} \ , \tag{5.16}$$

where ξ_+ is the correlation length of Eq. (2.51). Huber makes the reasonable assumption that $k_{\min} \approx 2\pi/L$ where L is a typical dimension of the system and that $k_{\max} \approx 2\pi/\xi_+$. Using Eqs. (5.15) and (5.16) to evaluate the integral he reports

$$D = 2^{-3/2} \left[\frac{\hbar}{m} \right] \left[\ln \left[\frac{L}{\xi_+ (1+\pi^2)^{1/2}} \right] \right]^{1/2} \ . \tag{5.17}$$

Though Eq. (5.17) theoretically increases as $T \to T_c$ and seems to predict the correct order of magnitude, we did not have an independent determination of ξ_+ nor did we understand how this theory applied to $T < T_{KT}$. Furthermore, assuming reasonable values for ξ_+ (see Sec. IV B), our measured D diverges much more strongly than predicted by Eq. (5.17), see Fig. 24.

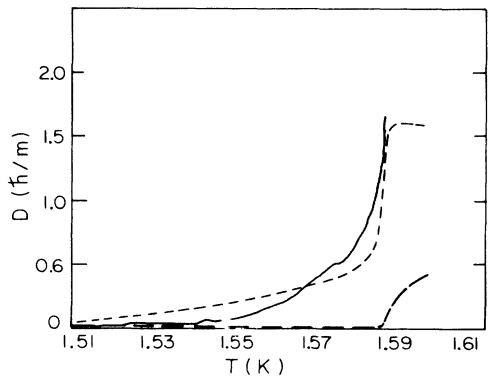

FIG. 24. Solid line—diffusivity measurement for a 14-Å film. Short-dashed line—prediction of Eq. (5.9) from AHNS analyses. Long-dashed line—prediction of Eq. (5.17) from Huber's analyses.

Finally, Petschek and Zippelius[36] have calculated the effect of bound pairs on D and predict that D should be renormalized downwards from its "bare" value D_0 as roughly $D_0/\tilde{\epsilon}$. Either this prediction is wrong or else our data reflects a rapid variation in D_0, unaccounted for in their theory.

We believe that the AHNS analysis is qualitatively correct and that diffusivity arises from the fluctuating velocity field of the vortex plasma via the fluctuation-dissipation theorem $D \propto \langle \eta^2 \rangle$ where η is a Gaussian noise source acting on a test vortex. As the plasma is heated, pairs in the vicinity of this test vortex become larger and more numerous, thereby increasing the magnitude of η which in turn contributes to D. Thus except for some small background contribution from rotons, phonons, and/or substrate, D seems to be a manifestation of the nature of the phase transition.

E. Characterization of data

We have made an unsuccessful attempt to find a functional dependence of D which collapses all of our data onto a single curve. This conflicts with Kim and Glaberson's[27] report that $D \propto (T/\sigma_s)^2$, independent of film thickness. Their experiment, however, was complicated by the fact that their films had a thickness which was a relatively strong function of temperature. They also only reported measurements over a rather small range of T_c's and were unable to measure D significantly above T_{KT}. Our data does, however, suggest that D diverges via a power law in reduced temperature. Shown in Fig. 25, is a log-log plot of D versus the inverse of the reduced temperature $(T_c - T)/T_c$ for several film thicknesses. The upper curves are for the thinnest films and have a slope of ~ 1. The behavior of the lower curves is much more rapid and may be a consequence of vortex pinning. Thus it appears that, in thin films, D diverges as $[T_c/(T_c - T)]$. This temperature dependence also seems to be consistent with the nonlinear superfluid dissipation data of Gillis *et al.*[20] They measure the onset of nonlinear dissipation in a Helmholtz resonator, operating at $\omega \sim 6000$ rad/sec, and numerically integrate a set of modified recursion relations for which D is varied to fit their data. Their measurements fall in the range $T/T_{KT} < 0.5$ ($T_{KT} \sim 1.2$ K) and are best fit with $D \sim 0.01\hbar/m$ at $T/T_{KT} \sim 0.3$. Given that T_{KT} is typically about 5 mK below T_c, this value of D is quite close to what one would predict by extrapolation from our high-temperature data.

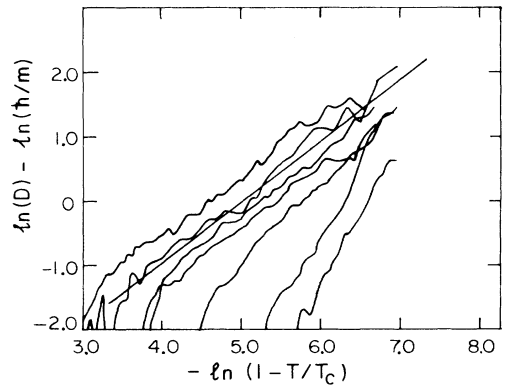

FIG. 25. The log of the diffusivity plotted as a function of the log of the reduced temperature. The upper curves are for the thinnest films. The solid line has unity slope to aid the eye.

F. Local finite amplitude effects

We have considered the possibility that the behavior of our rotational data does not entirely represent a temperature dependence in D. It is not unreasonable to assume that pairs in the vicinity of a free vortex are "stretched" by its local velocity field, thus increasing the average pair separation at all temperatures. Since the cold side of the dissipation peak arises from pairs with $r \sim r_D$, this effect could cause a widening of the peak similar to what we observe. We have used the finite flow recursion relations of Gillis *et al.*[20] to estimate the magnitude of this effect. This was done by calculating $\Delta Q^{-1}(\bar{v})$, where $\bar{v}$ is the velocity field of an arbitrary rotation induced vortex,

$$v(\xi) = \frac{\hbar}{m\xi} - \xi\Omega \ , \tag{5.18}$$

where ξ is the distance from its core. The flow induced dissipation was then averaged over the extent of the field

$$\overline{\Delta Q^{-1}}(v) = \frac{1}{A_v} \int_{r_D/2}^{r_\Omega} 2\pi\xi \Delta Q^{-1}[v(\xi)] d\xi \ , \tag{5.19}$$

where $r_\Omega \sim \sqrt{n_\Omega}$ is the interline spacing, r_D is the diffusion length, and $A_v = \pi(r_\Omega^2 - r_D^2)$. The lower limit of the integral reflects the fact that only pairs with separation of order r_D give rise to dissipation and that these pairs cannot be closer than $r_D/2$ to a rotation vortex. This calculation predicts a widening of the peak which is an order of magnitude smaller than what we observe, see Fig. 26. It also does not account for the extent of the rotating dissipation tail. We therefore believe that we were indeed measuring diffusivity.

G. Free vortex density of a rotating plasma

It is important to demonstrate that the free energy, $F = E - \Omega L$, of a rotating 2D vortex plasma is minimized

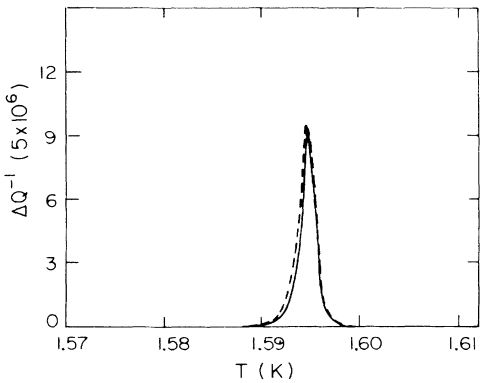

FIG. 26. Predicted widening of the peak due to local finite flow of rotation-induced vorticity.

by introducing the free vortex density n_Ω given by Eq. (2.80),

$$n_\Omega = \frac{m\Omega}{\pi\hbar} \ . \tag{5.20}$$

The analyses of our data assumes that n_Ω is given by this expression and that there is no net rotation induced polarization. We will first consider the case of a rotating film in which $T < T_{KT}$ and $n_\Omega = 0$. If we take $V_s(r)$ to be the average superfluid velocity in the rotating frame, then for temperatures well below T_{KT}, for which $\tilde{\epsilon} \approx 1$,

$$V_s(r) \approx -\Omega r \ , \tag{5.21}$$

where r is the radial distance from the axis of rotation. In general, however, Eq. (2.35) predicts that the superfluid will rotate as a solid body at a frequency less than Ω

$$V_s(r) = -\Omega r/\tilde{\epsilon} \ , \tag{5.22}$$

where $\tilde{\epsilon}$ is the *static* dielectric constant of the film (rotation induces dc flow). The free energy of the system is minimized when $V_s = 0$ in the rotating reference frame, which according to Eq. (5.22) cannot occur by polarization of the plasma alone. Therefore, free vorticity must be allowed to enter the system. To see that the equilibrium density of this rotation induced vorticity is, in fact, given by Eq. (5.20) we will consider an electric charge analog of the vortex plasma.

Consider a cylindrical dielectric with infinite azimuthal extent having a dielectric constant ϵ. In equilibrium, this cylinder contains many randomly oriented dipoles and no net polarization or polarization charge density. Now introduce a uniform background charge density ρ_b. The effect of the background charge is to induce a screening polarization charge. The analogy is the following (except for the detail of the directions)[16]:

$$\begin{aligned} &\mathbf{E} \leftrightarrows \mathbf{V}_s \\ &\frac{\rho_b}{2\epsilon_0} \leftrightarrows \Omega \ , \end{aligned} \tag{5.23}$$

where $\mathbf{E}$ is the electric field and ϵ_0 is permittivity of free space. The electrostatic equations determining the polarization $\mathbf{P}$ and displacement field $\mathbf{D}$ are

$$\nabla \cdot \mathbf{P} = -\rho_p \ , \tag{5.24}$$

$$\nabla \cdot \mathbf{E} = (\rho_b + \rho_p)/\epsilon_0 \ , \tag{5.25}$$

$$\mathbf{D} = \epsilon_0 \mathbf{E} + \mathbf{P} \ , \tag{5.26}$$

$$\mathbf{D} = \epsilon\epsilon_0 \mathbf{E} \ , \tag{5.27}$$

where ρ_p is the polarization charge density. Equations (5.26) and (5.27) imply that

$$\mathbf{P} = \epsilon_0(\epsilon - 1)\mathbf{E} \ , \tag{5.28}$$

where

$$\mathbf{E} = \frac{\rho_b r \hat{\mathbf{r}}}{2\epsilon\epsilon_0} \tag{5.29}$$

inside the cylinder. The analog of allowing vortices to freely enter and move through the film is to allow a nonzero conductivity, σ, in the dielectric. Since the free-charge contribution to ϵ is proportional to σ/ω, where ω is the frequency of the applied field, it is obvious that, at dc, free charges give rise to an infinite dielectric constant which implies no electric field, polarization, or polarization charge in the cylinder. The free charges brought in from the outside must have a density such as to just cancel ρ_b, which in the vortex formalism, is equivalent to Eq. (5.20).

Implicit in all of this discussion is the assumption that the free-energy minimum vortex density is obtained in our experimental situation. Because we never observed hysteresis with respect to rotation and because we observed the same excess dissipation whether we began rotating at low temperatures and warmed through the transition or began the experimental run by rotating at high temperatures (e.g., above the λ point), we are convinced that the rotation induced vortex density was indeed its equilibrium value.

VI. CONCLUSION

In summary, we have made direct measurements of vortex diffusivity, a parameter of crucial importance in describing the dynamical 2D phase transition as well as in interpreting thermal conductance experiments, and observe a rather strong divergence at T_c. This divergence suggests that the dynamics of the phase transition itself are responsible for the diffusivity. No adequate theory now exists which fully accounts for the observed behavior.

*Present address: AT&T Bell Laboratories, Murray Hill, NJ 07974.

[1]D. R. Nelson, *Phase Transitions* (Academic, London, 1983), Vol. 7.
[2]J. M. Kosterlitz and D. J. Thouless, J. Phys. C **6**, 1181 (1973).
[3]D. R. Nelson and J. M. Kosterlitz, Phys. Rev. Lett. **39**, 1201 (1977).
[4]V. Ambegaokar and S. Teitel, Phys. Rev. B **19**, 1667 (1979).
[5]V. Ambegaokar, B. I. Halperin, D. R. Nelson, and E. D. Siggia, Phys. Rev. Lett. **40**, 783 (1978).
[6]P. W. Adams and W. I. Glaberson, Phys. Rev. Lett. **57**, 82 (1986).
[7]F. Block, Z. Phys. **61**, 206 (1930).
[8]R. Peierls, Ann. Inst. Henri Poincare **5**, 177 (1935).
[9]P. C. Hohenberg, Phys. Rev. **158**, 383 (1967).
[10]E. Long and L. Meyer, Phys. Rev. **79**, 1031 (1950); **85**, 1030 (1952).
[11]R. Bowers, D. F. Brewer, and K. Mendelssohn, Philos. Mag. **42**, 1445 (1951).
[12]C. W. Everitt, K. R. Atkins, and A. Denenstein, Phys. Rev. **136**, A1494 (1964).
[13]I. Rudnick, Phys. Rev. Lett. **40**, 1454 (1978).
[14]D. J. Bishop and J. D. Reppy, Phys. Rev. Lett. **40**, 1727 (1978).
[15]W. I. Glaberson and R. J. Donnelly, in *Progress in Low Temperature Physics*, edited by D. F. Brewer (North-Holland, Am-

sterdam, 1986), Vol. IX.
[16]V. Ambegaokar, B. I. Halperin, D. R. Nelson, and E. D. Siggia, Phys. Rev. B **21**, 1806 (1980).
[17]J. P. McCauley, J. Phys. C **10**, 689 (1977).
[18]B. A. Huberman, R. J. Myerson, and S. Doniach, Phys. Rev. Lett. **40**, 780 (1978).
[19]J. S. Langer and J. D. Reppy, *Progress in Low Temperature Physics* (North-Holland, Amsterdam, 1967), Vol. 6, p. 1.
[20]K. A. Gillis, S. Volz, and J. M. Mochel, J. Low Temp. Phys. **61**, 172 (1985).
[21]H. E. Hall and W. F. Vinen, Proc. Phys. Soc., London, Sect. A **238**, 215 (1958).
[22]P. W. Adams, M. Cieplak, and W. I. Glaberson, Phys. Rev. B **32**, 215 (1985).
[23]H. E. Hall, Proc. R. Soc. London, Ser. A **245**, 546 (1958).
[24]D. J. Bishop and J. D. Reppy, Phys. Rev. B **22**, 5171 (1980).
[25]G. Agnolet, S. L. Teitel, and J. D. Reppy, Phys. Rev. Lett. **47**, 1537 (1981).
[26]D. Finotello and F. M. Gasparini, Phys. Rev. Lett. **55**, 2156 (1985).
[27]M. Kim and W. I. Glaberson, Phys. Rev. Lett. **52**, 53 (1984).
[28]E. L. Andronikashvili, Zh. Eksp. Teor. Fiz. **16**, 780 (1946).
[29]D. J. Bishop (private communication).
[30]Approximately 10–20 % of the temperature dependence of σ_s^0 arose from desorption of the film. This effect was implicitly absorbed into the variation of h_T and did not affect the quality of the fits.
[31]A. T. Fiory, A. F. Hebard, and W. I. Glaberson, Phys. Rev. B **28**, 5075 (1983).
[32]J. Maps and R. B. Hallock, Phys. Rev. B **27**, 5491 (1983).
[33]The decrease in $D(T_{KT})$ with increasing film thickness has also been observed in thin-film superconductors. See A. F. Hebard and M. A. Paalanen, Phys. Rev. Lett. **54**, 2155 (1985).
[34]D. L. Huber, Phys. Lett. **79A**, 331 (1980).
[35]J. B. Taylor and B. McNamara, Phys. Fluids **14**, 1492 (1971).
[36]R. G. Petschek and A. Zippelius, Phys. Rev. B **23**, 3483 (1981).